

**Relative Permeability and the Microscopic Distribution of  
Wetting and Nonwetting Phases in the  
Pore Space of Berea Sandstone\***

E.M. Schlueter,<sup>†‡</sup> P.A. Witherspoon,<sup>†</sup> N.G.W. Cook,<sup>†‡</sup> and L.R. Myer<sup>†</sup>

*† Earth Sciences Division  
Lawrence Berkeley Laboratory  
University of California  
Berkeley, California 94720*

*and*

*‡ Department of Materials Science and Mineral Engineering  
University of California, Berkeley*

April 1994

---

\*This research was supported by the U.S. Department of Energy through the Assistant Secretary for Fossil Energy, Bartlesville Project Office, Advanced Extraction Process Technology (AEPT), under contract No. DE-AC22-89BC14475, and by the Director, Office of Energy Research, Office of Basic Energy Sciences, Engineering and Geosciences Division, under Contract No. DE-AC03-76SF00098.

**MASTER**

# Relative Permeability and the Microscopic Distribution of Wetting and Nonwetting Phases in the Pore Space of Berea Sandstone

E.M. Schlueter,<sup>†‡</sup> P.A. Witherspoon,<sup>†</sup> N.G.W. Cook,<sup>†,‡</sup> and L.R. Myer<sup>†</sup>

<sup>†</sup>*Earth Sciences Division  
Lawrence Berkeley Laboratory  
University of California  
Berkeley, California, 94720*

and

<sup>‡</sup>*Department of Materials Science and Mineral Engineering  
University of California, Berkeley*

## ABSTRACT

Experiments to study relative permeabilities of a partially saturated rock have been carried out in Berea sandstone using fluids that can be solidified in place. The effective permeability of the spaces not occupied by the wetting fluid (paraffin wax) or the nonwetting fluid (Wood's metal), have been measured at various saturations after solidifying each of the phases. The tests were conducted on Berea sandstone samples that had an absolute permeability of about 600 md. The shape of the laboratory-derived relative permeability vs. saturation curves measured with the other phase solidified conforms well with typical curves obtained using conventional experimental methods. The corresponding wetting and nonwetting fluid distributions at different saturations are presented and analyzed in light of the role of the pore structure in the invasion process, and their impact on relative permeability and capillary pressure. Irreducible wetting and nonwetting phase fluid distributions are studied. The effect of clay minerals on permeability is also assessed.

## I. INTRODUCTION

Relative permeability and its associated capillary pressure effects are relevant to problems such as enhanced oil recovery and waste remediation and/or isolation. About 50% or more of the original oil-in place is left in a typical U.S. oil reservoir by traditional primary and secondary (i.e., water-flooding) techniques.<sup>[1]</sup> This unrecovered oil is a large target for enhanced or tertiary oil recovery methods that are being developed.

The concept of relative permeability comes into play in the extension of Darcy's law from single phase flow to the multiphase realm.<sup>[2]</sup> It is generally assumed that relative permeabilities of immiscible fluids are only functions of saturation. A great number of experimental investigations<sup>[3,4,5]</sup> substantiate this assumption within limits. For example, Terwilliger and Yuster<sup>[6]</sup> and later Calhoun<sup>[7]</sup> found that the chemical compositions of the fluids do not matter much, and that the relative permeability functions are approximately the same for any "wetting-nonwetting" fluid system. This is a direct consequence of the fact that the microstructure of reservoir rocks strongly influences the mobilization and distribution of fluids in the pore space. Moreover, such factors as (1) fluid/fluid properties—interfacial tension (IFT), viscosity ratio, density difference, phase behavior, and interfacial mass transfer; (2) fluid/solid properties—wettability, ion exchange, adsorption, and interaction; and (3) magnitude of applied pressure gradient, gravity, and aging have been found to play roles in interpreting the motion and distribution of oil in petroleum reservoirs.<sup>[8,9]</sup>

The relative permeabilities are empirical coefficients which appear in the continuum form of Darcy's law for two-phase flow through porous media:

$$\frac{q_w}{A} = \frac{k_{rw}k}{\mu_w} \frac{dp_w}{dx} \quad (1)$$

$$\frac{q_{nw}}{A} = \frac{k_{rnw}k}{\mu_{nw}} \frac{dp_{nw}}{dx} \quad (2)$$

where  $q_w$  and  $q_{nw}$  are the volumetric flowrates of the wetting and nonwetting phases,  $\mu_w$  and  $\mu_{nw}$  are the viscosities of those phases,  $dp_w/dx$  and  $dp_{nw}/dx$  are the macroscale pressure gradients in those phases, and  $A$  is the cross-sectional area, perpendicular to the flow, of the porous medium. The parameters  $k_{rw}k$  and  $k_{rnw}k$  are the permeabilities to the wetting and nonwetting phases;  $k$  is the permeability of the porous medium when only one phase is present, and  $k_{rw}$  and  $k_{rnw}$  are the wetting and nonwetting phase relative permeabilities. The relative permeabilities depend upon wetting-phase saturation,  $S_w$ —the fraction of pore volume occupied by the wetting phase. The nonwetting phase saturation,  $S_{nw}$ , is determined from  $S_{nw} = 1 - S_w$ .

As Eqs. (1) and (2) show, the relative permeability factor is an empirical representation of a well-defined transport process in a highly complex pore space geometry and topology. In spite of this complexity, simplified mathematical models of the pore structure have been proposed.<sup>[10,11,12]</sup> However, such parameters as pore-body and pore-throat distributions, pore coordination numbers and individual fluid-phase coordination numbers as a function of saturation, which are implemented in the mathematical models, have not been determined experimentally. This is due in part to the lack of good experimental techniques required for visualizing three-dimensional (3-D) microstructures in natural porous media while maintaining the original pore and phase geometry.

Therefore, we decided to work on this problem with several main objectives in mind: (1) to further develop an experimental technique initiated by Yadav et al.<sup>[13]</sup> that would allow measurement of relative permeability for the full range of saturation, (2) to visualize directly 2-D pore structure and wettabilities for the full range of saturation, (3) to interpret experimental data and fluid distributions qualitatively and quantitatively with respect to pore geometry and topology, (4) to evaluate relative permeability data in terms of microphysics and microchemistry of the processes involved (i.e., effect of clay minerals coating pores), and (5) to compare our results to relative permeability and associated capillary pressure experimental data obtained using conventional methods.

## II. APPARATUS AND PROCEDURE

The apparatus that was used in this study was designed to simultaneously measure both hydraulic and electrical conductivity<sup>[14]</sup> (Figure 1). The rock core (5 cm in diameter and 5 cm in length) is encased in a rubber jacket and placed in the test cell. The test cell base is connected directly to the bottom of the sample, and a centrally-located orifice is attached to allow fluids to flow through the mounted core. A confining pressure of 50 psi (3.4 atm) is applied using nitrogen gas. Fluid flow through the core is controlled by a syringe pump that provides constant flow rates. The basic procedure used for measuring permeability is first to vacuum saturate each core completely with triple-distilled water. Distilled water is then pumped through the core, and flow is continued for a sufficient time to establish constant pressure readings. It was found that about four pore volumes of water are required to achieve steady state. In our experiments, we used samples of Berea sandstone, which is a homogeneous sedimentary rock used as a reference rock in the petroleum industry. The intrinsic permeability and porosity of a Berea sandstone core are about 600 md ( $600 \times 10^{-15} \text{ m}^2$ ) and 22%, respectively. It is estimated to be of Mississippian age and is found in Berea, Ohio.

### III. EFFECT OF PARTIAL WETTING PHASE SATURATION

To determine the effect of partial fluid saturation on permeability, we utilized Berea sandstone samples that had been permeated with triple-distilled water and measured the single phase hydraulic conductivity. The samples were then oven dried. This procedure was applied to every sample to find the permeability before paraffin application. Some samples also had electrical conductivity measured. The samples were then partially filled with paraffin wax at controlled saturations of 20%, 30%, 40%, 50%, 60%, and 70%. Paraffin wax is a wetting phase composed of a mixture of solid hydrocarbons of high molecular weight with a density of  $0.76 \text{ g/cm}^3$ , a dynamic viscosity of about  $3 \times 10^{-3} \text{ Pa}\cdot\text{s}$  at  $150^\circ\text{C}$ , and a melting point of  $56^\circ\text{C}$ . The paraffin is applied at temperatures higher than its melting point in the core axial direction, until uniform saturation is achieved throughout the sample (Figure 2). The paraffin is then solidified in place at ambient temperature conditions. After paraffin application, the rock grain surfaces became hydrophobic. To measure the effective permeability, the rock samples that were partially saturated with paraffin were permeated with distilled water. The effective permeability of the pore spaces not occupied by the wetting fluid as a function of paraffin saturation is presented in Figure 3 (Case A). Experiments in which electrical conductivity was not measured previous to paraffin impregnation were also carried out; the results are shown in Figure 3 (Case B). In summary, good agreement, within experimental error, was found between the two sets of experiments A and B.

Note that the extrapolated value of permeability at zero paraffin saturation from Figure 4 - Case B ( $\sim 600 \text{ md}$ ) is higher than the measured value of permeability obtained at the same saturation when using triple-distilled water ( $\sim 300$  to  $400 \text{ md}$ ) (Table I). A possible explanation of this phenomenon is given in section IV.

#### A. Effect of pore structure and topology

To understand how pore structure and topology control permeability, the hydraulic conductivity data (Figure 4) have been studied in light of the wetting-fluid distributions at each saturation regime (Figures 5 to 7) with the aid of a complete rock pore cast (Figure 8) and its associated rock section (Figure 9). The rock pore cast was obtained from a rock specimen that had been fully impregnated with Wood's metal alloy and the quartz grains removed by hydrofluoric acid. The rock pore cast and its associated rock section clearly reveal that the pore space is composed of grain-contact porosity (e.g., thin sheets and micropores) and intergranular porosity. Paraffin imbibition occurs because surface tension effects encourage the displacing fluid to advance. The overall dynamics of the wetting phase imbibition process is as

follows: In the grain-contact pore space, in the smaller throats, and in the surface capillary grooves, capillary pressure is high, and the paraffin will advance quickly to the next pore. The pores exert much less capillary pressure, and for a given pressure difference between the phases only the smaller pores will fill. Once a pore is filled, the paraffin will next fill all throats leading from it, again rapidly. A new set of pores will be reached and the process continues. Therefore, during paraffin imbibition the flow dynamics are pore-dominated.

Figure 5 shows a scanning electron microscope (SEM) photomicrograph collage of a Berea sandstone specimen that has been partially saturated with approximately 20–30% paraffin. The gray phase corresponds to quartz grains, the white phase corresponds to pores that have been impregnated with paraffin, and the black phase corresponds to the remaining pore space, which was filled with blue epoxy for imaging purposes. Paraffin has invaded grain-contact pore space (i.e., thin sheets and micropores) and intergranular pore space connected by smaller throats, but has only coated the available intergranular channels connected by larger throats. A minor effect on effective permeability is observed (Figure 4). Therefore, the fraction of the pore structure connected by smaller constrictions (e.g., grain-contact pore space) do not contribute much to effective permeability. Figure 6 shows an SEM photomicrograph collage of a rock specimen partially saturated with approximately 40–50% paraffin. At this stage, we are filling main intergranular conduits connected by the larger throats. A substantial effect on effective permeability is observed. Figure 7 shows an SEM photomicrograph collage of a rock specimen partially saturated with approximately 60–70% paraffin. We have filled almost all intergranular conduits connected by larger throats. A few intergranular pores not well connected still remain unfilled. When paraffin saturation is  $\sim 70\%$ , the whole pore structure behaves as though hydraulically disconnected. Results are summarized in Table II.

### **B. Irreducible wetting phase saturation**

Overall, it is observed that the wetting phase at low saturations is confined to a continuous network of conduits throughout the porous medium (Figure 5). It is composed of clusters of intergranular pores, edges, corners and wedges of intergranular pores, capillary channels present on rough surfaces of pores, and single grain-contact pores. Since the wetting fluid at low saturations forms a hydraulically connected continuum, it is possible to reduce the wetting phase saturation progressively, at least in principle. Therefore, the “irreducible wetting phase saturation” is not constant and becomes a function of capillary pressure.

Thus, the existence of the “irreducible wetting phase saturation” in a consolidated rock such as Berea sandstone is due to the fact that (1) grain-contact pores have

narrow throats and large surface area, (2) pores have corners (angular cross sections), and (3) the pore surface is rough at the microscopic scale (Figure 10) leading to strong capillary forces which tend to trap the wetting phase.

#### IV. EFFECT OF CLAY MINERALS

X-ray diffraction studies by Khilar and Fogler,<sup>[15]</sup> in conjunction with scanning electron microscopy (Figures 11 to 13) and energy-dispersive x-ray analysis (Figure 14), indicate that Berea sandstone contains  $\sim 8\%$  by weight of dispersable and swelling clays (mainly kaolinite with some illite and smectite), 80% quartz, and 12% feldspar. The injection of a fluid such as triple-distilled water whose solution chemistry is not compatible with the porous rock in its natural state can bring significant reductions in the permeability. This is a manifestation of peptization and flocculation of clay particles due to the water sensitivity of Berea sandstone. Khilar and Fogler<sup>[15]</sup> found that when flow is switched from salt water to fresh water, clay particles are released from the pore wall. The particles then migrate in the direction of the flow and are trapped at throats which results in blockage of the pores of the sandstone, decreasing the permeability. For electrolyte solutions with cations of valence 1, at  $\text{pH} = 7$ , a critical salt concentration (0.07 M for sodium chloride solution at  $30^\circ\text{C}$ ) has been found below which clay particles are released from Berea sandstone pore walls.<sup>[15]</sup> Particle migration is thought to be the most important mechanism in water-sensitive Berea sandstone due to the fact that the amount of swelling clays is minimal. The peptization and flocculation of clay particles due to the water sensitivity of Berea sandstone may be explained in terms of double-layer theory. The major forces that hold the clay particles to the pore walls are the London-van der Waals forces of attraction. The forces causing the detachment of the clay particles are the double-layer forces of repulsion and possibly, under conditions of high flow rate, hydrodynamic shear. Calculations show the two forces of double-layer repulsion and hydrodynamic shear to be the most probable cause for particle release.<sup>[16]</sup> Experimental observations<sup>[15]</sup> strongly suggest that the double-layer force of repulsion may be the dominant cause of particle release. These observations include the two most important parameters that govern the stability of the colloidal suspension of clay particles: temperature and type of cation. More importantly, the phenomenon occurs only at relatively low salt concentration, where the double-layer repulsive forces are large.

It is important to recognize that the clay minerals present in the rock have been immobilized by coating pores with hydrocarbon paraffin. Therefore, the permeability extrapolated to paraffin saturation of zero (i.e., no hydrocarbon paraffin) corresponds to either the permeability of the clean rock without clays or the permeability of the rock with clay, but with brine as flowing fluid (with concentration above critical salt

concentration if monovalent cations are employed). This hypothesis was verified by partially removing clays in a Berea sandstone core by acid treatment with a mixture of 6% hydrochloric and 1.5% hydrofluoric acids (Suarez-Rivera, personal communication, 1991). After the core was treated and clays flushed out, the permeability was found to be 574 md using triple-distilled water, higher than the measured permeability values obtained when using triple-distilled water on untreated cores ( $\sim 300$  to 400 md) (Table I).

## V. EFFECT OF PARTIAL NONWETTING PHASE SATURATION

In this experimental investigation, we have examined the relationship between the microscopic pore occupancy of a nonwetting fluid and its effect on effective permeability and capillary pressure.

We have used three-dimensional imbibition of a nonwetting Wood's metal alloy instead of the conventional mercury porosimetry. This technique offers the advantage of allowing analysis of the occupied pore space after the experiment. Wood's metal is an alloy of about 43% Bi, 38% Pb, 11% Sn, and 9% Cd, with a specific gravity of 9.6, a viscosity of about  $1.3 \times 10^{-3}$  Pa·s at 75°C, and a surface tension of about 400 mN/m.<sup>[13]</sup> The setup for the three-dimensional imbibition experiments is shown in Figure 15. It consists of a metallic container of Wood's metal placed in a metal vacuum chamber provided with a lucite window and surrounded by a heating element to keep the metal molten (melting point varies from about 50°C to 70°C depending on its composition). A micrometer is attached to the metallic container to determine the pressure at which the Wood's metal first enters the specimen. The 5 cm-long and 5 cm-diameter sandstone sample is first oven-dried, and then immersed in the molten Wood's metal in the metallic container and placed in the metal vacuum chamber. Then the sample is de-aired by applying a full vacuum for about 60 minutes, until no air bubbles are observed through the lucite window. A subatmospheric pressure is applied by drawing a partial vacuum, which is maintained at the desired value by a regulating valve until capillary equilibrium is achieved. Each sample was allowed to imbibe at a fixed equilibrium pressure for approximately 90 minutes, until no movement of Wood's metal was noticed through the lucite window. At a pressure of about 5 to 6 psia, the micrometer signaled the first indication of Wood's metal entering the pore space (probably an edge effect on the sample sides). The capillary pressure experiment was repeated on several samples by applying pressure externally under quasistatic conditions in the range of approximately 6 to 14 psia. The imbibed samples were cut into four axial quarters each of which had a different saturation. To minimize the effect of gravity (hydrostatic) gradient, we took the top quarter of each imbibed specimen at a particular equilibrium pressure and measured its saturation.

Figure 16 shows the Wood's metal imbibition curve where the volume of Wood's metal intruded (normalized by the total pore volume) is plotted vs. the applied pressure. Fluid saturation increases rather sharply with a corresponding small increase in capillary pressure in the saturation range from about 10 to 50%. Our result is consistent with typical capillary pressure curves based on conventional mercury porosimetry saturation for Berea (BE-1) sandstone (Figure 17).<sup>[12]</sup> Berea (BE-1) sandstone has almost the same macroscopic properties as the Berea sandstone we used in our experiments (e.g., porosity of 22%, permeability to N<sub>2</sub> of 400 md, and a formation factor of 15.5). After Wood's metal application, the rock samples were vacuum-saturated and permeated with triple-distilled water to measure the effective permeability (Table III). Figure 18 shows the effective permeability curve of the spaces not occupied by the nonwetting fluid, measured at various saturations (in a Berea sandstone of absolute permeability of ~ 600 md).

#### A. Effect of pore structure and topology

To understand how pore structure and topology control the physical property under consideration, we have studied the effective permeability and capillary pressure data in light of the nonwetting fluid distributions observed at each equilibrium pressure. For this purpose, optical and scanning electron microscopic examinations of the tops of samples (after cutting off 3 mm) have provided valuable insights into the pore-level complexity of the natural porous media. In the Wood's metal imbibition process, some external pressure is needed to overcome surface tension and push the Wood's metal through the pores and throats. Large throats, with their comparatively weak capillary pressures, will fill more readily than small throats. Once the fluid reaches a pore, capillary pressure is reduced, and the pore will fill rapidly. In this process, the flow dynamics are mainly controlled by the throats. Isolated regions will occur because a region of large throats surround a region of constricted throats.

Figure 19 shows an optical photograph of the nonwetting fluid distributions obtained in top axial quarters in the pressure range 6.8 to 7.7 psia. It is observed that the nonwetting fluid flow network is composed of a set of imbibing clusters correlated in space. At every pressure step, the nonwetting fluid resides in the pores accessible through throats with a radius larger than that corresponding to the current equilibrium capillary pressure. As the pressure increases, the nonwetting phase saturation increases, and the nonwetting fluid invades successively smaller pores and becomes connected to regions which were previously separated from this phase by small throats. At 6.8 psia (Figure 19), the fluid has preferentially penetrated the sample sides. The saturation is greatest near the perimeter of the sample, and least at the center. This observation suggests that pores near the cylindrical surface of the sample are bet-

ter connected than those towards the center. This interconnection could arise from exposure of pores where they intersect the surface, or from damage adjacent to this surface. At 6.9 psia (Figure 19), a saturation gradation is observed in the direction of flow at this pressure (preferentially horizontal). The longer flow paths are connected by smaller constrictions, so fewer flow channels are going to the sample center starting from all available channels at the sample surface. At pressures of 7.2 psia (Figure 19) and greater, the nonwetting fluid invades more and more smaller pores, becoming connected to regions that were separated from this phase by smaller pores, and the clusters of nonwetting phase become larger and larger. Figure 20 shows an SEM photomicrograph collage of a 1 in  $\times$  1 in rock specimen saturated with about 30% Wood's metal at 7.2 psia equilibrium pressure. Large percolating clusters have been formed. An SEM photomicrograph collage of an enlarged partial section from the last figure (Figure 21) show that there are relatively few intergranular conduits connected by larger throats filled with the nonwetting phase. At this stage, a substantial effect on effective permeability is observed. Figure 22 shows an SEM photomicrograph collage of a 1 in  $\times$  1 in rock specimen saturated with approximately 50% of Wood's metal at 8.5 psia equilibrium pressure. Smaller percolating clusters are observed. An SEM photomicrograph collage of an enlarged partial section from the last figure and its associated pore contours areas (Figure 23), show that there are still many large (intergranular) pore segments connected by small throats that do not contribute to the flow of the nonwetting phase in the rock. In addition, the grain contact pore space (i.e., thin sheets and micropores) does not contribute either. Furthermore, simple statistical analysis of pore contour areas obtained from Figure 23 has shown that relatively few conduits connected by large intergranular throats carry up to about 50% of the nonwetting fluid in the porous media under consideration, producing a clustered structure. At this stage, the effective permeability is almost zero. Thus, we have found that a large percentage of the permeability of the medium is contributed by a relatively small number of intergranular conduits connected by larger throats of narrow size distribution and of high hydraulic conductance. The effect of nonwetting phase saturation on effective permeability is summarized in Table IV.

### **B. Irreducible nonwetting phase saturation**

In contrast to the previously discussed "irreducible wetting phase saturation", it is observed that the trapped clusters of a nonwetting fluid are separate entities that are not hydraulically interconnected with each other (Figure 7). We have found that when the wetting phase saturation is about 70%, the effective permeability is zero. Thus the nonwetting fluid simply ceases to flow when its saturation falls below the irreducible nonwetting phase saturation limit ( $\sim 30\%$ ) because its continuity breaks

down, leaving isolated stranded clusters of disconnected fluid.

## VI. RESULTS AND DISCUSSION

Experimental studies have been conducted aimed at studying permeability of a partially saturated rock. For this purpose, the effective permeabilities of the spaces not occupied by the wetting fluid (paraffin wax) and the nonwetting fluid (Wood's metal), respectively, have been measured at various saturations, while solidifying the other phase. The experiments were conducted in Berea sandstone samples of  $\sim 600$  md absolute permeability. The absolute permeability was extrapolated from the effective permeability curve after partially filling the rock pore space with paraffin. The extrapolated value of permeability at zero paraffin saturation ( $\sim 600$  md) is higher than the measured value of permeability obtained at the same saturation when using triple-distilled water ( $\sim 300$  to  $400$  md). A possible explanation is that the paraffin immobilizes the effect of clay present in the rock pore space (e.g., prevents clay migration, swelling, etc.).

The relative permeabilities,  $k_r$ , obtained as a ratio of effective permeability to absolute permeability of the rock, are shown in Figure 24. The wetting phase relative permeability is concave upward while the nonwetting phase relative permeability has an *S* shape. The shape of the nonwetting phase relative permeability in the steep-sloped zone indicates that for a small reduction in nonwetting phase (increase in wetting phase) there is a relatively large decrease in relative permeability. This rapid decrease is due to the occupation of larger pores or flow paths by the wetting phase. The nonwetting relative permeability curve reaches nearly 100% at a nonwetting phase saturation less than a 100% which means that part of the interconnected space composed by smaller pores (e.g., grain-contact) does not contribute to the nonwetting phase relative permeability of the porous medium (but does contribute to electrical conductivity).<sup>[14]</sup> The sum of the relative permeabilities is less than unity. One of the reasons is that part of the pore channels available for flow of a fluid may be reduced in size by the other fluid present in the rock. Another reason is that immobilized droplets of one fluid may completely plug some constrictions in a pore channel through which the other fluid would otherwise flow. The laboratory-derived relative permeability data conforms with *typical* relative permeability curves using oil and gas as the wetting and nonwetting phase, respectively, in Berea sandstone using conventional methods (Figure 25).<sup>[17]</sup> It is observed that the two curves have similar trends. The relative permeabilities are nearly symmetric within the same range of saturation at which intergranular channels connected by larger throats control effective permeability. This observation then is consistent with fluid flow studies that show that when immiscible fluids flow simultaneously through a porous medium, each fluid

follows its own flow path.<sup>[18]</sup> When Darcy's law is applied to the measurement of relative permeabilities of immiscible fluids, it is assumed that the interfaces are steady, the phases flow through their respective channels as if the other phase were absent, and each fluid phase obeys Darcy's law. These conditions are met in the application of this technique. Thus, it is possible to measure the macroscopic properties using only single-phase experiments, while the other phase is frozen in place. It is worth noting that strong phase interference has been found experimentally for the relative permeability function (e.g.,  $k_{rw} + k_{rnw} \ll 1$ ) for a 3-D porous media. Moreover, the fluid phases are allowed to flow together in a rather narrow range of saturation.

The capillary pressure curve obtained when partially saturating the rock with the nonwetting phase (Wood's metal) is presented in Figure 16. Our result is consistent with *typical* capillary pressure curves based on conventional mercury porosimetry saturation for Berea sandstone (Figure 17). The initial portion of the curve with positive curvature is interpreted as being associated with surface defects. The rapid rise in the curve occurs when the intruded Wood's metal initially forms a connected cluster. Thereafter, there is a sharp increase in fluid saturation with a corresponding small increase in capillary pressure due to the narrow distribution of pore-throat sizes. In our previous work on Berea sandstone capillary pressure function and its relationship to microgeometry,<sup>[19]</sup> we have used a simple functional form to determine average pore and throat sizes controlling capillary pressure and relative permeability. Our result, assuming a lognormal distribution of pore sizes, gave a narrow distribution of intergranular pore-throats represented by a hydraulic radius  $R_{H_m} = 6.6 \mu\text{m}$ , and a standard deviation  $\sigma = 0.14$ . The corresponding nonwetting fluid distributions are presented in Figure 16. It is found that the flow network is composed of spatially correlated percolating clusters. As the nonwetting phase saturation reduces, the network for this phase breaks down and becomes discontinuous and hydraulically disconnected. Thus, the irreducible nonwetting phase saturation,  $S_{rnw}$ , is found to have a value of about 30% (percolation threshold). In contrast, since the wetting phase constitutes a continuous network even at low wetting phase saturations, the irreducible wetting phase saturation becomes a function of capillary pressure (e.g.,  $S_{rw} \ll 30\%$ ).

## VII. CONCLUDING REMARKS

The permeability of a partially-saturated rock is controlled by the rock structure and topology as well as the physics and chemistry of mineral-fluid interactions. To understand the relationships, we have measured the effective permeability in the pore spaces not occupied by a wetting fluid (paraffin wax), or a nonwetting fluid, after solidifying the fluid in place. It is important to recognize that when the rock is par-

tially saturated with the hydrocarbon paraffin, the clay minerals present in the rock pore space are immobilized. Thus, permeability extrapolated to paraffin saturation of zero,  $k \approx 600$  md, corresponds to the permeability of the "clean" rock (e.g., without clay). Effective permeability data have been studied in light of the fluid distributions observed at different saturations with the aid of a complete pore cast and its associated rock section. Our analysis shows that (1)  $\sim 30\%$  of the pore space consists of grain-contact pores (i.e., thin sheets and micropores) and intergranular pores connected by smaller throats, (2)  $\sim 40\%$  of the pore space comprises intergranular conduits composed of pores connected by larger throats, and (3)  $\sim 30\%$  of the intergranular pore space remains hydraulically disconnected. The grain-contact pore space of large surface areas (thin sheets), micropores, and intergranular pores connected by smaller throats provide only minor alternate paths for the fluid to flow compared to the intergranular conduits connected by larger throats.

On the basis of our experimental observations of the relationship between microscopic nonwetting fluid occupancy and the fluid distributions and of their effect on capillary pressure of Berea sandstone, we have found that relatively small number of intergranular channels connected by large throats of narrow size distribution are responsible for conducting a relatively large amount of the nonwetting fluid through the medium (at least in the saturation range up to approximately 50%). In fact, we have also found that a large percentage of the permeability of the medium is contributed by a relatively small number of conduits connected by large intergranular throats of narrow size distribution and high hydraulic conductance.

### VIII. ACKNOWLEDGEMENTS

This work was supported by the U.S. Department of Energy through the Assistant Secretary for Fossil Energy, Bartlesville Project Office, Advanced Extraction Process Technology (AEPT), under contract No. DE-AC22-89BC14475, with the University of California at Berkeley. Additional funding was provided by the Director, Office of Energy Research, Office of Basic Energy Sciences, Engineering and Geosciences Division, under contract No. DE-AC03-76SF00098 with the Lawrence Berkeley Laboratory. Thanks are due to Christine Doughty and Robert Zimmerman of Lawrence Berkeley Laboratory for a careful review of the manuscript. The authors thank Robin Curtis of Lawrence Berkeley Laboratory for technical assistance with the experimental equipment, and Ron Wilson of U.C. Berkeley for assistance with the scanning electron microscope.

---

*REFERENCES*

- <sup>1</sup>Reserves of crude oil, natural gas liquids, and natural gas in the U.S. and Canada as of December 31, 1977. American Petroleum Institute, 32, (1978).
- <sup>2</sup>Scheidegger, A.E. 1974. *The Physics of Flow through Porous Media*. University of Toronto Press.
- <sup>3</sup>Hassler, G.L., Rice, R.R., and Leeman, E.H. 1936. Investigations of recovery on the oil from sandstones by gas-drive. *Transactions AIME*, 118, p.116.
- <sup>4</sup>Wyckoff, R.D. and Botset, H.G. 1936. Flow of gas liquid mixtures through sands. *Physics*, 7, p.325.
- <sup>5</sup>Botset, H.G. 1940. Flow of gas liquid mixtures through consolidated sands. *Transactions AIME*, 136, p.91.
- <sup>6</sup>Terwilliger, P.L., and Yuster, S.T. 1946. *Producers Monthly* 11(1), p.42. 1947 *Oil Weekly* 126(1), p.54.
- <sup>7</sup>Calhoun, J.C. 1951. *Oil and Gas J.* 50(21), p.117. 1951b *Oil and Gas Journal* 50(20), p.308.
- <sup>8</sup>Dullien, F.A.L. 1979. *Porous Media Fluid Transport and Pore Structure*. Academic Press.
- <sup>9</sup>Stegemeir, G.L. 1977. *Mechanism of Entrapment and Mobilization of Oil in Porous Media. Improved Oil Recovery by Surfactant and Polymer Flooding*. D.O. Shah and R.S. Schechter (eds.), Academic Press.
- <sup>10</sup>Fatt, I., and Dykstra, H. 1951. *Relative Permeability Studies*. *Transactions AIME* 192, p.249.
- <sup>11</sup>Rose, W., and Witherspoon, P.A. 1956. *Studies of Waterflood Performance: II. Trapping Oil in a Pore Doublet*. *Producers Monthly* 21(2), p.32.
- <sup>12</sup>Chatzis, I., and Dullien, F.A.L. 1977. Modelling pore structure by 2-D and 3-D networks with application to sandstones. *Journal of Canadian Petroleum Technology* 16, p.97.
- <sup>13</sup>Yadav, G.D., Dullien, F.A.L., Chatzis, I., and Macdonald, I.F. 1987. *Microscopic*

distribution of wetting and nonwetting phases in sandstones during immiscible displacements. SPE Reservoir Engineering, May, p.137.

- <sup>14</sup>Schlueter, E., Myer, L.R., Cook, N.G.W., and Witherspoon, P.A. 1993. Formation factor and the microscopic distribution of wetting phase in pore space of Berea sandstone. Lawrence Berkeley Laboratory Report LBL-33207. *In* Proceedings of the Society of Exploration Geophysicists, 63rd Annual International Meeting, Washington, D.C., September 26-30, p.1245.
- <sup>15</sup>Khilar, K.C., and Fogler, H.S. 1984. The existence of a critical salt concentration for particle release. *Journal of Colloid Interface Science* 101, p.214.
- <sup>16</sup>Mungan, N. 1968. Permeability reduction due to salinity changes. *Journal of Canadian Petroleum Technology*, 7(8), p.113.
- <sup>17</sup>Corey, A.T., and Rathjens, C.H. 1956. Effect of stratification on relative permeability. *Transactions AIME*, 207, p.358.
- <sup>18</sup>Honarpour, M., Koederitz, L., and Harvey, A.H. 1986. *Relative Permeability of Petroleum Reservoirs*. CRC Press, Inc.
- <sup>19</sup>Schlueter, E.M., Zimmerman, R.W., Myer, L.R., Cook, N.G.W., and Witherspoon, P.A. 1994. Predicting the capillary pressure function of Berea sandstone from microgeometry. *In* Proceedings of the 8th International Conference of the Association for Computer Methods and Advances in Geomechanics, Morgantown, West Virginia, May 22-28.

TABLE I. Effective (and absolute) permeability data (Case B) - Berea sandstone partially saturated with paraffin wax, with triple-distilled water used as permeant.

| Sample | $S_w^a$ (%) | $k_{eff}^b$ (md) | $k_{abs}^c$ (md) |
|--------|-------------|------------------|------------------|
| 1EB4   | 16          | 513              | 282              |
| 1EB2   | 24          | 553              | 329              |
| S-1R   | 24          | 501              | 333              |
| 1EB3   | 32          | 489              | 376              |
| 1EB5   | 32          | 473              | 296              |
| 1EB6   | 41          | 206              | 463              |
| 1EB1   | 44          | 121              | 288              |
| S-3R   | 50          | 54               | 391              |
| KS15   | 69          | 15               | —                |

<sup>a</sup> Paraffin wax saturation.

<sup>b</sup> Effective permeability.

<sup>c</sup> Absolute permeability.

TABLE II. WETTING FLUID INVASION AND PERMEABILITY

- $0.0 \leq S_w \leq 0.3$

Wetting fluid fills well-connected grain contact pore space (e.g., thin sheets and micropores) and intergranular conduits connected by smallest throats, while only coating available intergranular pore space connected by larger throats.



Very small effect on effective permeability.

- $0.3 < S_w \leq 0.5$

Wetting fluid fills to partially-fills few intergranular conduits connected by large throats.



Very large effect on effective permeability.

- $0.5 < S_w \leq 0.7$

Wetting fluid fills remaining more tortuous intergranular conduits connected by large throats.



Smaller effect on effective permeability.

- $0.7 < S_w \leq 1.0$

Structure is disconnected, i.e., nonwetting phase is trapped in disconnected intergranular pore space.

TABLE III. Effective (and absolute) permeability data - Berea sandstone partially saturated with Wood's metal, with triple-distilled water used as permeant.

| Sample | $P_c^a$ (psia) | $S_{nw}^b$ (%) | $k_{eff}^c$ (md) | $k_{abs}^d$ (md) |
|--------|----------------|----------------|------------------|------------------|
| ESB5   | 6.8            | 5.2            | 280              | 346              |
| EMB3   | 6.9            | 7.7            | 242              | 388              |
| KBS11  | 7.2            | 26             | 45               | 386              |
| ESB3   | 7.3            | 32             | 19               | 345              |
| KBS9   | 7.7            | 42             | 0.71             | 319              |

<sup>a</sup> Capillary pressure.

<sup>b</sup> Wood's metal saturation.

<sup>c</sup> Effective permeability.

<sup>d</sup> Absolute permeability.

TABLE IV. NONWETTING FLUID INVASION AND PERMEABILITY

- $0.0 \leq S_{nw} \leq 0.2$

Nonwetting fluid fills few intergranular conduits connected by larger throats of narrow distribution. Large clusters are observed.



Very large effect on effective permeability.

- $0.2 < S_{nw} \leq 0.4$

Nonwetting fluid fills remaining more tortuous intergranular conduits connected by large throats of narrow distribution. Smaller clusters are observed.



Smaller effect on effective permeability.

- $0.4 < S_{nw} \leq 0.7$

Nonwetting fluid fills grain contact and intergranular pore space connected by smallest throats.



Very small effect on effective permeability.

- $0.7 < S_{nw} \leq 1.0$

When is structure disconnected?, i.e., wetting phase is coating connected intergranular pore space filled with the nonwetting phase and is present in intergranular pore space connected by smaller throats as well.

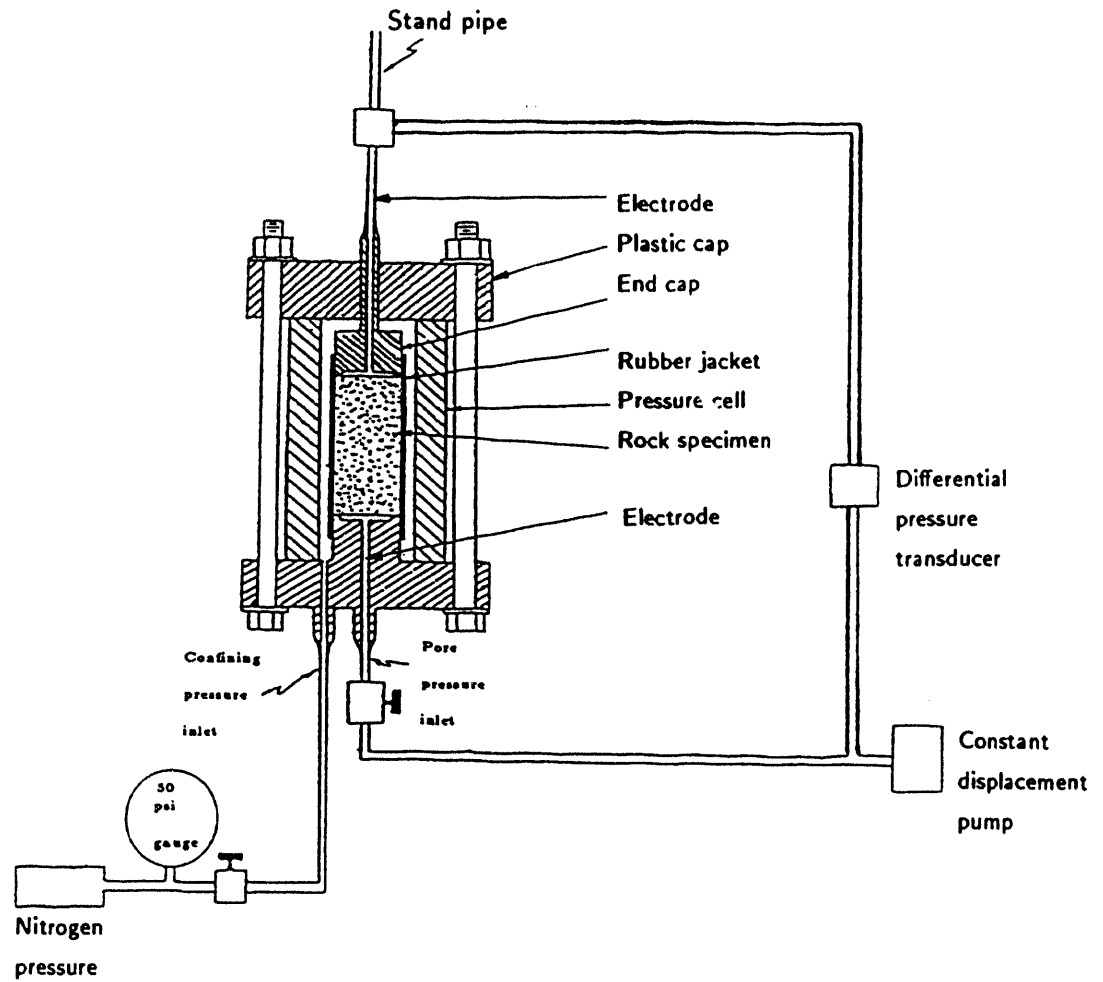


FIG. 1. Schematic representation of the laboratory apparatus designed to simultaneously measure both hydraulic and electrical conductivity.

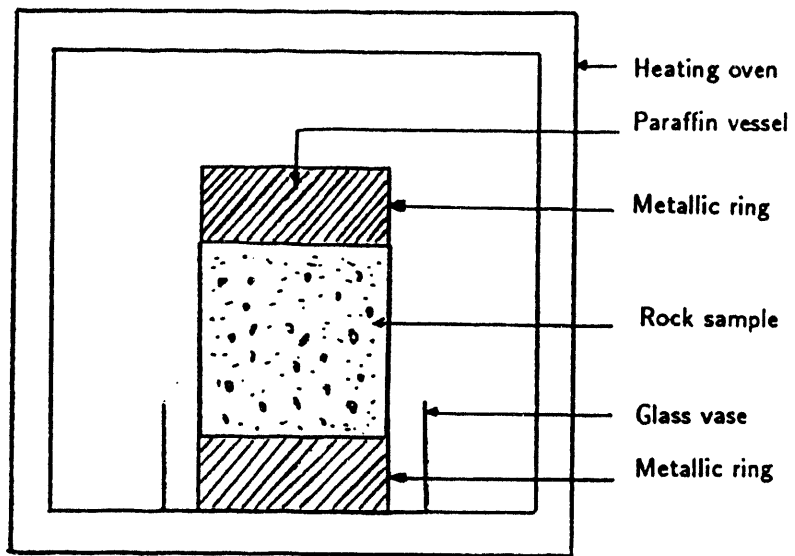


FIG. 2. Experimental setup for one-dimensional paraffin impregnation.

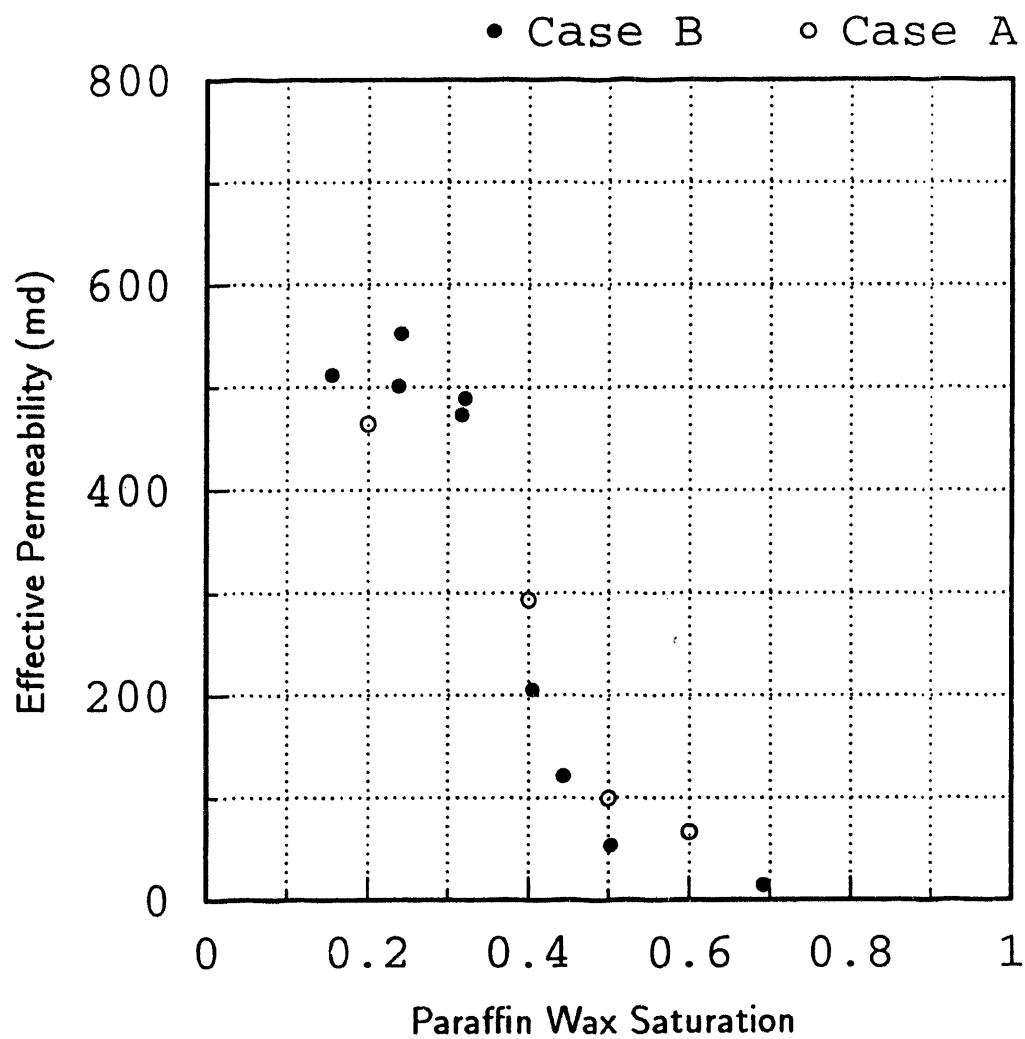


FIG. 3. Effective permeability vs. paraffin saturation for Berea sandstone. The pore space was partially saturated with hydrocarbon paraffin. The remaining portion of the pore space was filled with triple-distilled water. Cases A and B correspond to experimental data on samples subjected or not subjected to electrical conductivity measurement before paraffin application, respectively.

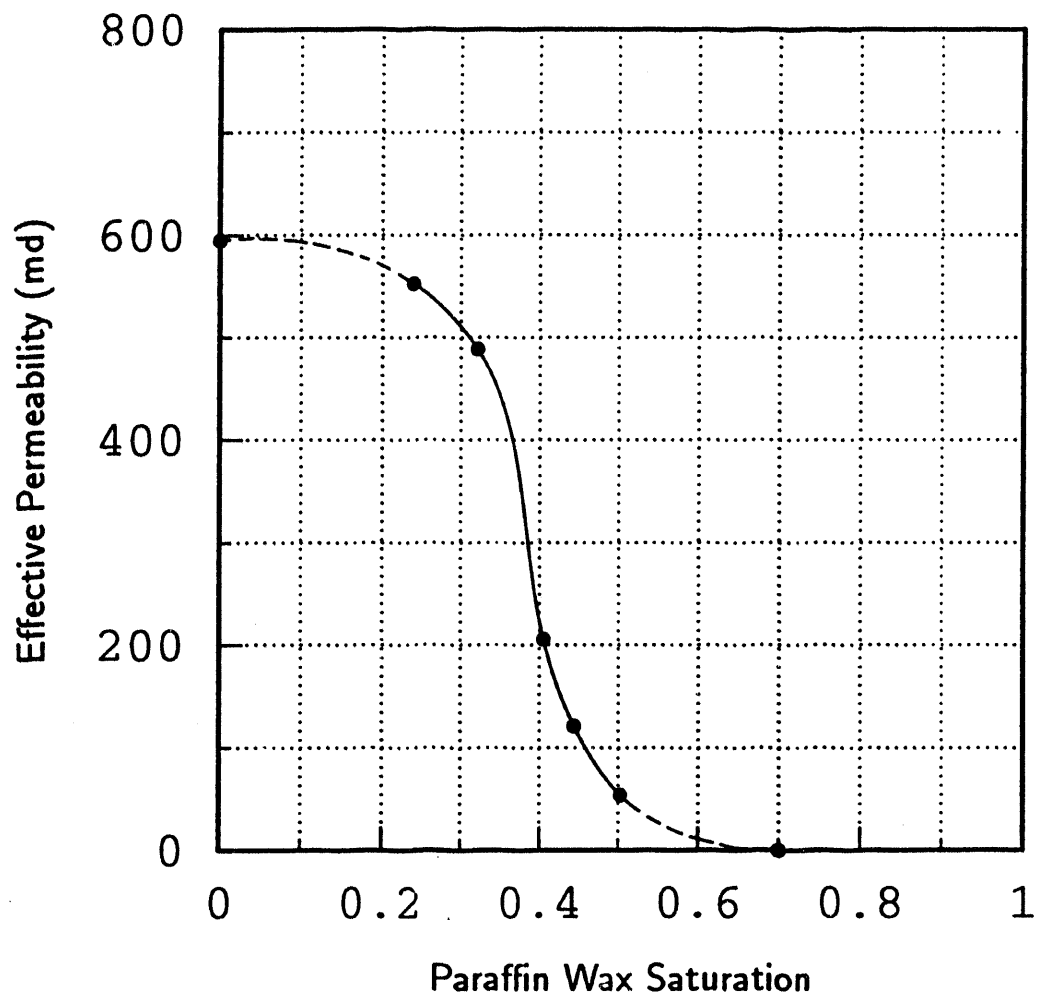
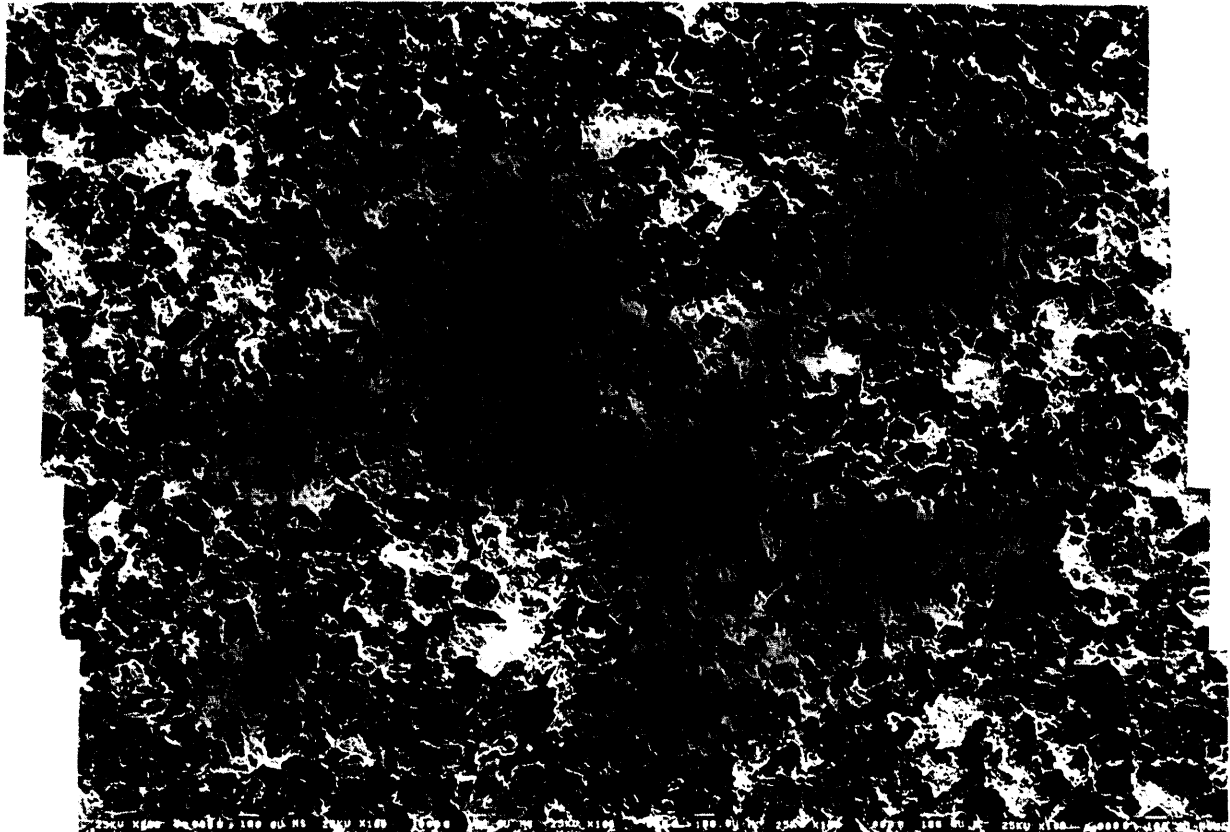
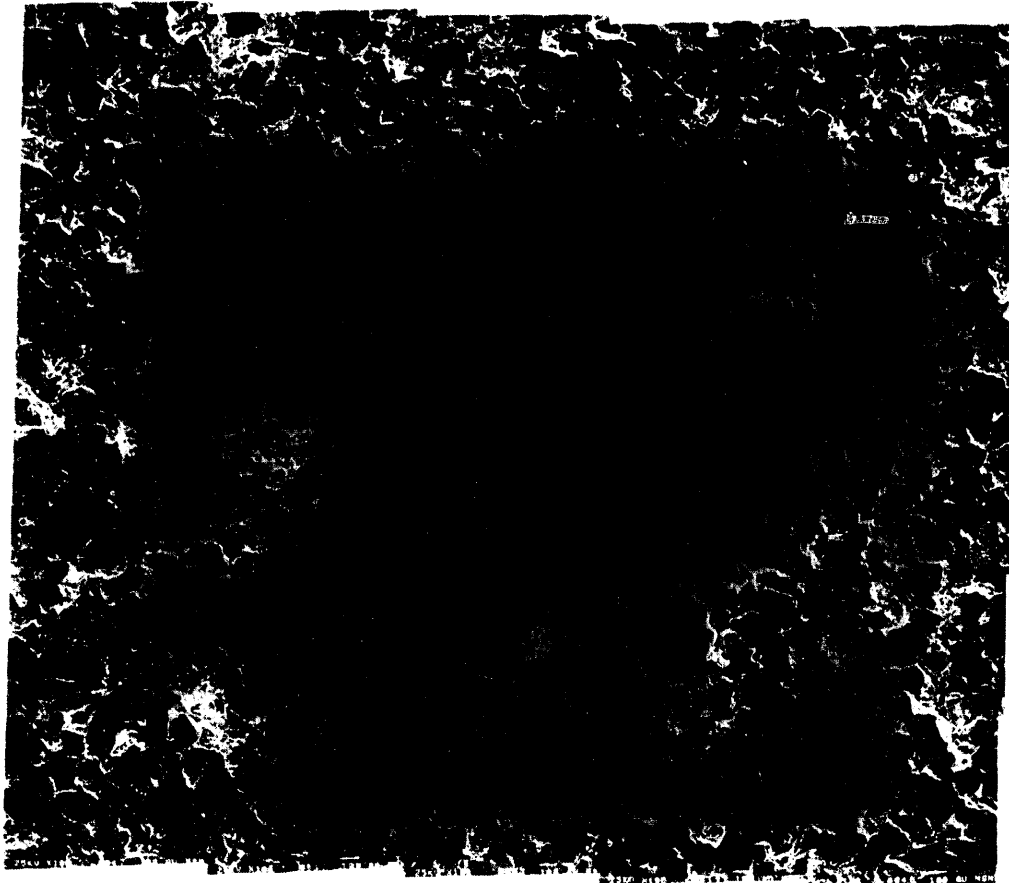


FIG. 4. Effective permeability vs. paraffin wax saturation for Berea sandstone (case B). The pore space was partially saturated with hydrocarbon paraffin, with the remainder of the pore space filled with triple-distilled water.



**FIG. 5.** SEM photomicrograph collage of a Berea sandstone specimen impregnated with approximately 20-30% paraffin. The actual width of field is about 6 mm. The gray phase represents quartz grains, the white phase represents pores saturated with paraffin, and the black phase represents remaining pores filled with blue epoxy for imaging purposes.



**FIG. 6.** SEM photomicrograph collage of a Berea sandstone specimen impregnated with approximately 40-50% paraffin. Actual width of field is about 6 mm. The gray phase represents quartz grains, the white phase represents pores saturated with paraffin, and the black phase represents remaining pores filled with blue epoxy for imaging purposes.

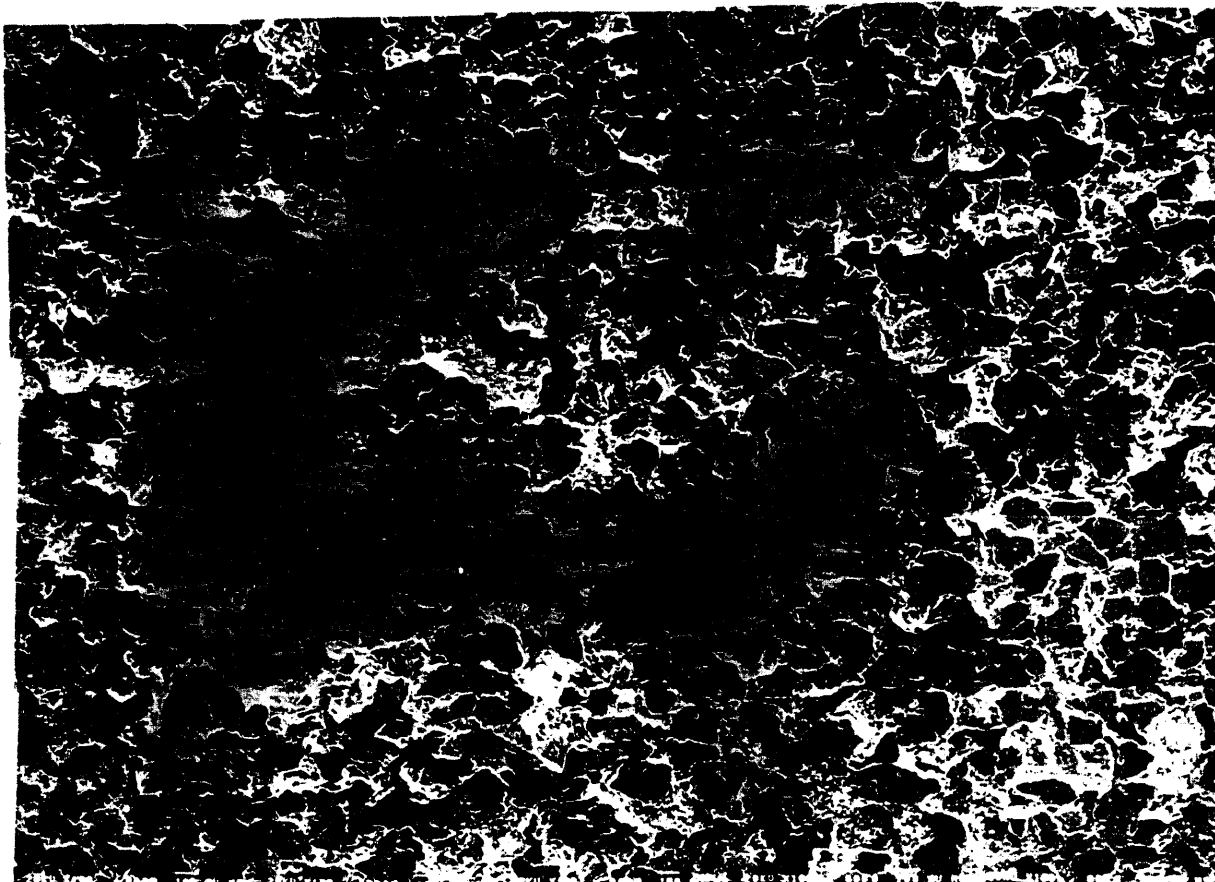


**FIG. 7.** SEM photomicrograph collage of a Berea sandstone specimen impregnated with approximately 60-70% paraffin. Actual width of field is about 6 mm. The gray phase represents quartz grains, the white phase represents pores saturated with paraffin, and the black phase represents remaining pores filled with blue epoxy for imaging purposes.

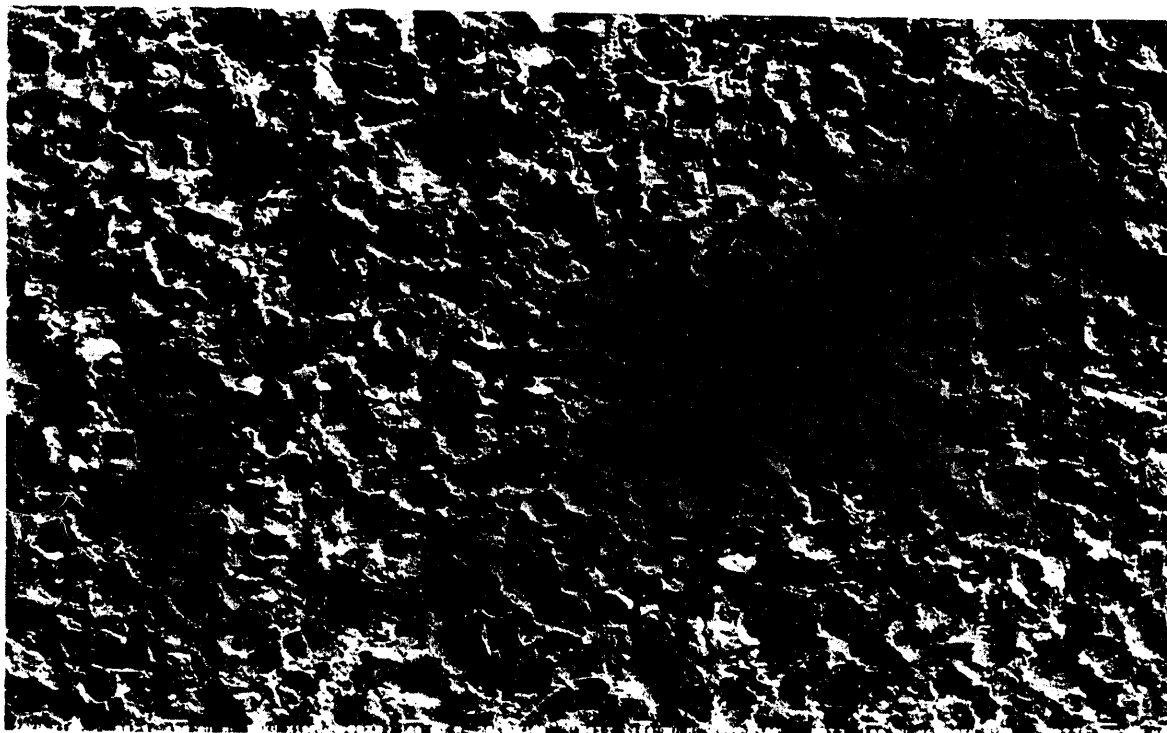


**FIG. 8.** SEM photomicrograph collage of a Berea sandstone pore cast. Actual width of field is about 6 mm. The rock pore space was completely filled with Wood's metal alloy and the quartz grains removed by hydrofluoric acid to allow direct observation of the pore structure.

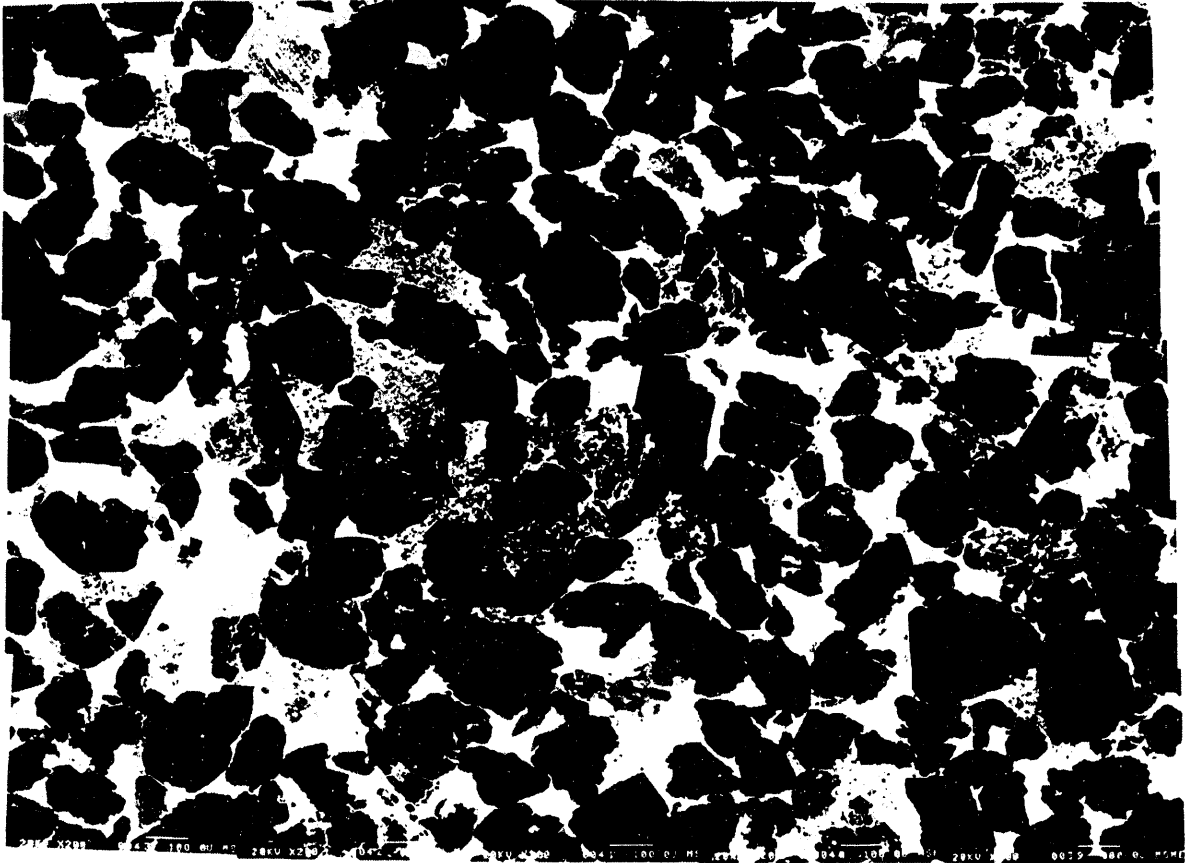


FIG. 9. SEM photomicrograph collage of a Berea sandstone sample fully impregnated with Wood's metal alloy. Actual width of field is about 3 mm. The gray phase is quartz grains, and the white phase is pores saturated with the alloy. The section reveals that the pore space is composed of grain-contact porosity (i.e., thin sheets and micropores) and intergranular porosity.



**FIG. 10.** Typical SEM photomicrograph collage of Berea sandstone showing pore-grain interface roughness. The rock is composed mainly of quartz grains (dark gray), feldspar grains (medium gray), and products of grain dissolution (light gray). The pore space is impregnated with Wood's metal alloy (white), and epoxy (black). Actual width of field is about 1.5 mm.

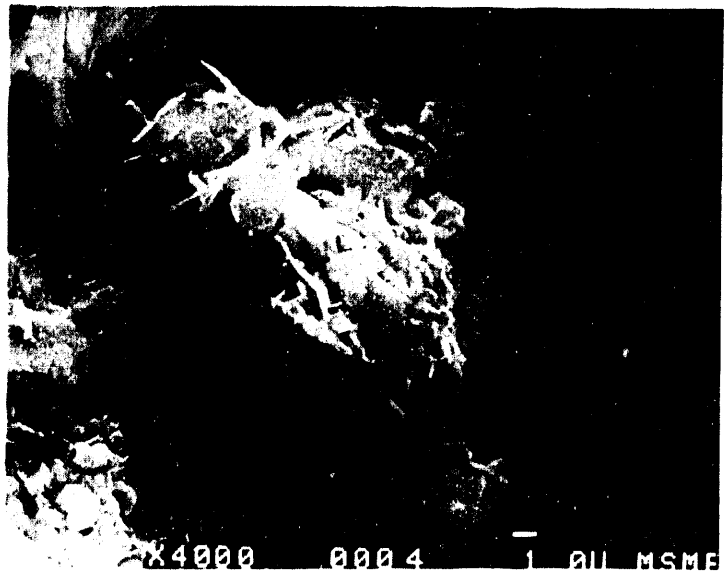
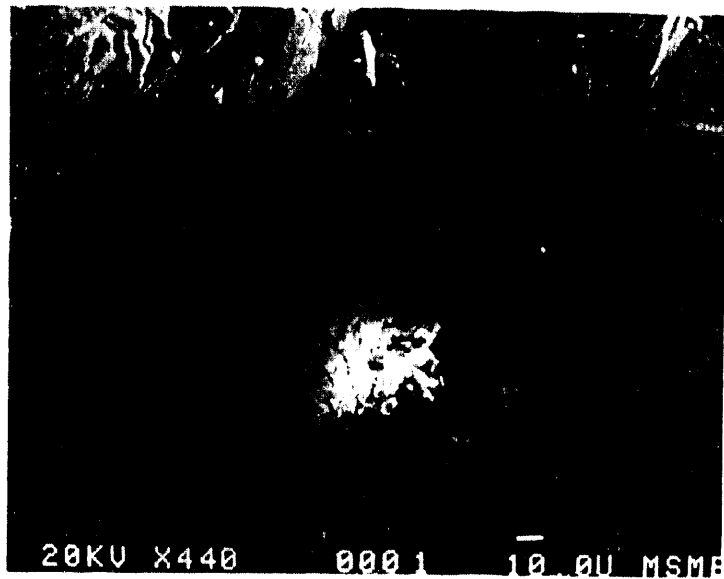


FIG. 11. SEM photomicrographs of a Berea sandstone specimen showing the presence of fine-grained clay minerals (mainly kaolinite) partly filling pores between quartz grains.



FIG. 12. SEM photomicrographs of a Berea sandstone specimen showing the presence of fine-grained clay minerals (mainly illite) partly filling pores between quartz grains.

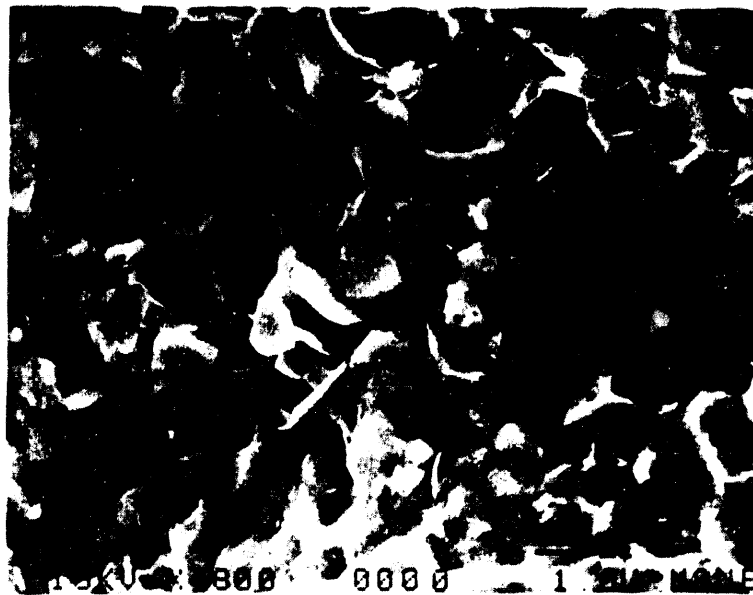


FIG. 13. SEM photomicrographs of a Berea sandstone specimen showing the presence of fine-grained clay minerals (mainly montmorillonite) partly filling pores between quartz grains.

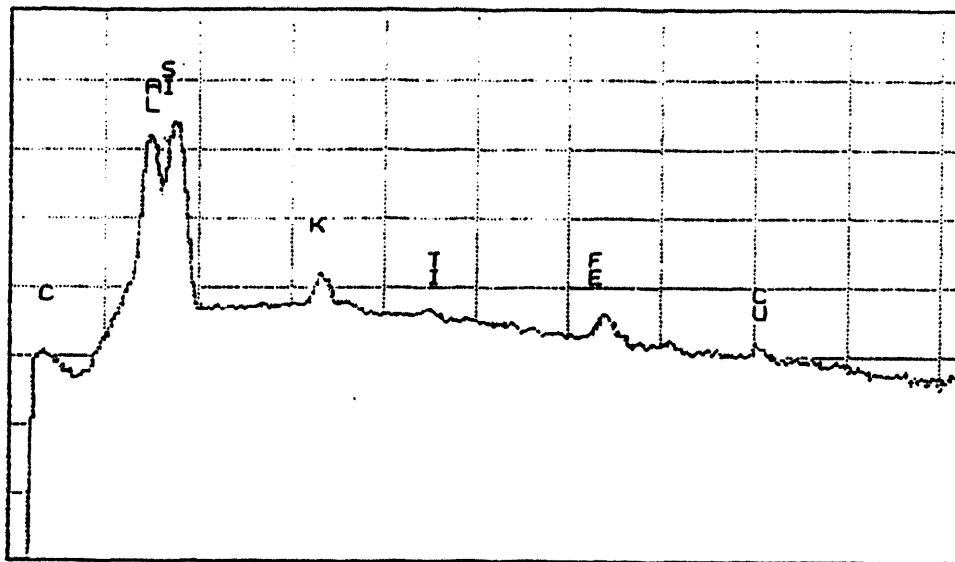


FIG. 14. X-ray spectrum of clay minerals coating Berea sandstone sample pores shown in figure 11. EDX analysis yielding nearly equal peak heights of Si and Al confirms the identification as kaolinite.

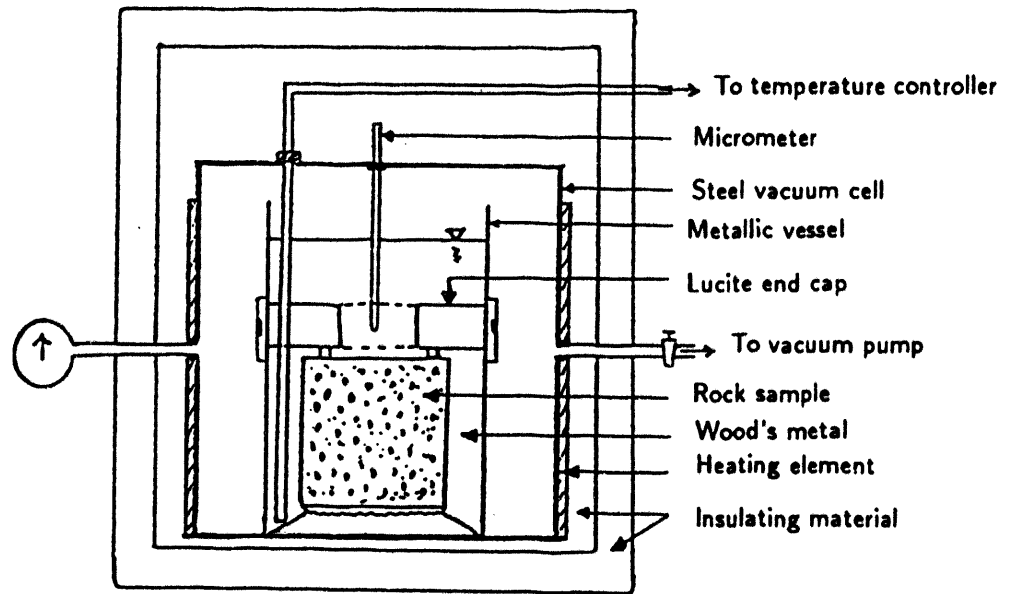


FIG. 15. Experimental setup for three-dimensional Wood's metal imbibition.

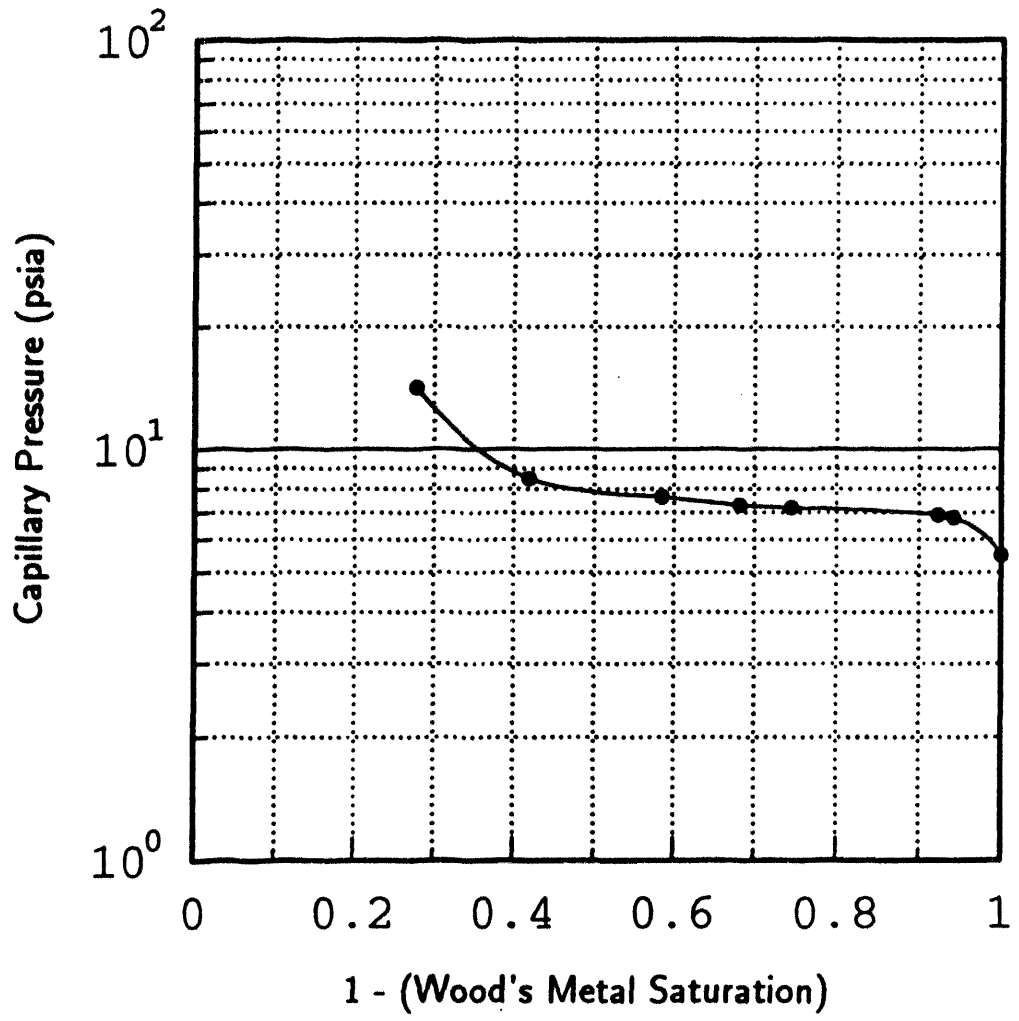


FIG. 16. Experimental capillary pressure function of Berea sandstone. The rock has been impregnated with a nonwetting fluid (Wood's metal) at different equilibrium pressures, and solidified in place. The procedure allows for direct observation and analysis of the fluid distribution at a fixed pore pressure and saturation level.

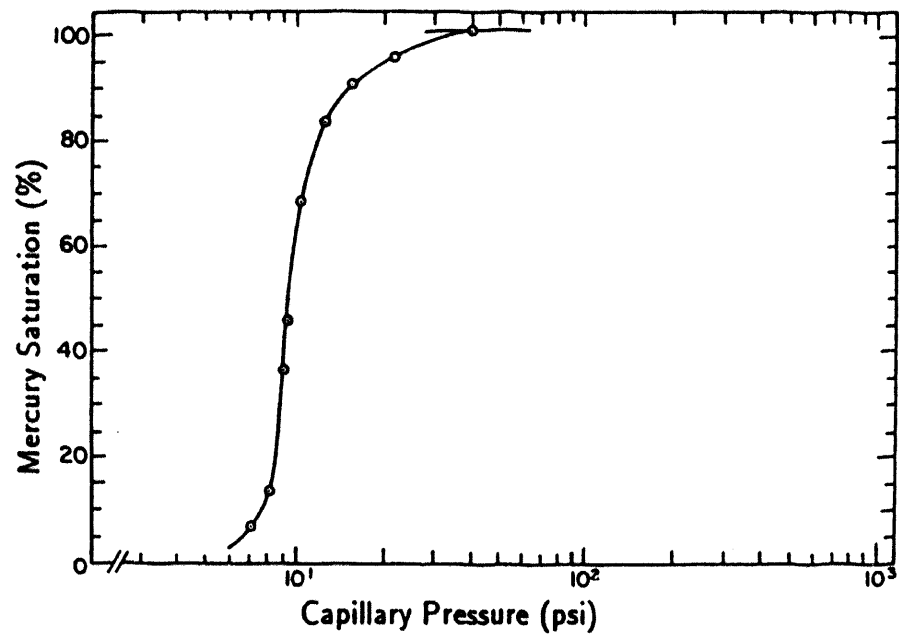


FIG. 17. Experimental mercury porosimetry saturation curve of Berea sandstone (after Chatzis and Dullien, 1977).

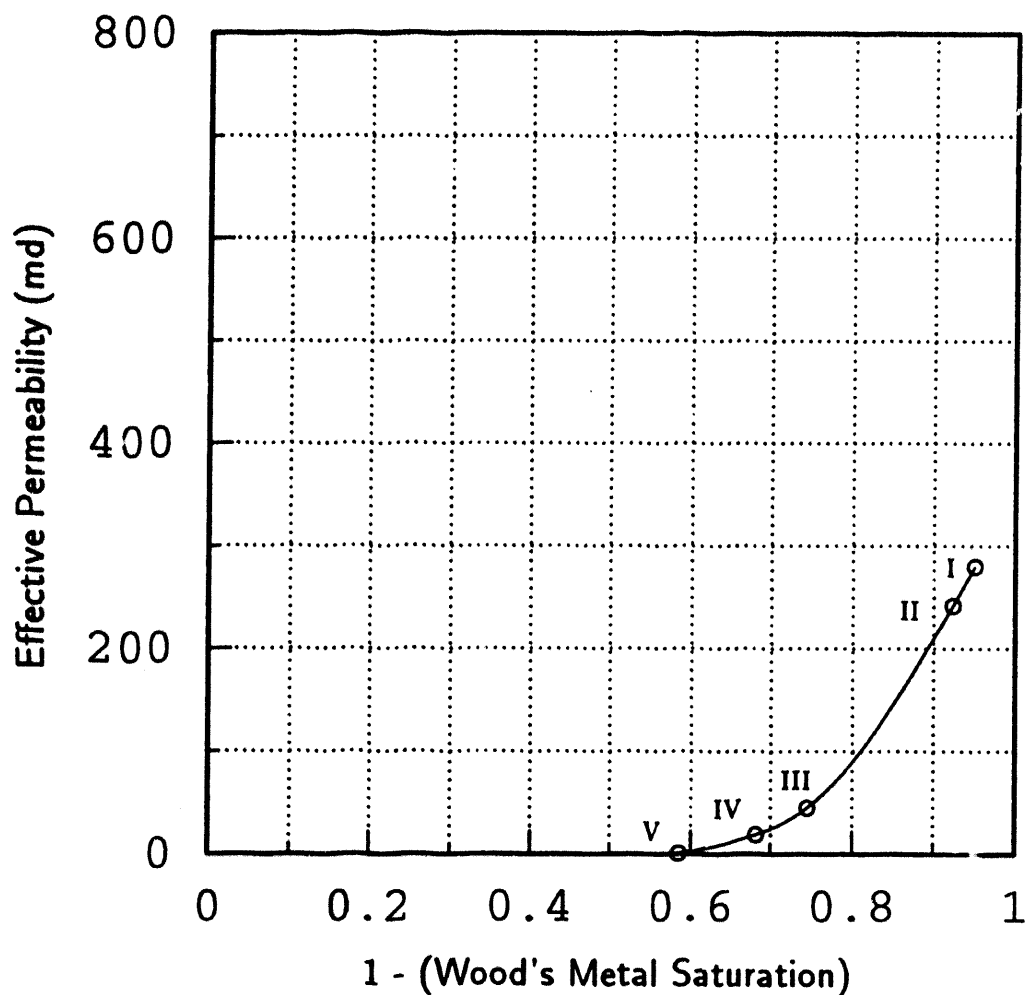


FIG. 18. Effective permeability vs. 1-Wood's metal saturation for Berea sandstone. The pore space was partially saturated with Wood's metal at different pressures, with the remainder of the pore space filled with triple-distilled water. The capillary pressures (in psia) for the points on the plot are I = 6.8, II = 6.9, III = 7.2, IV = 7.3, and V = 7.7 psia.

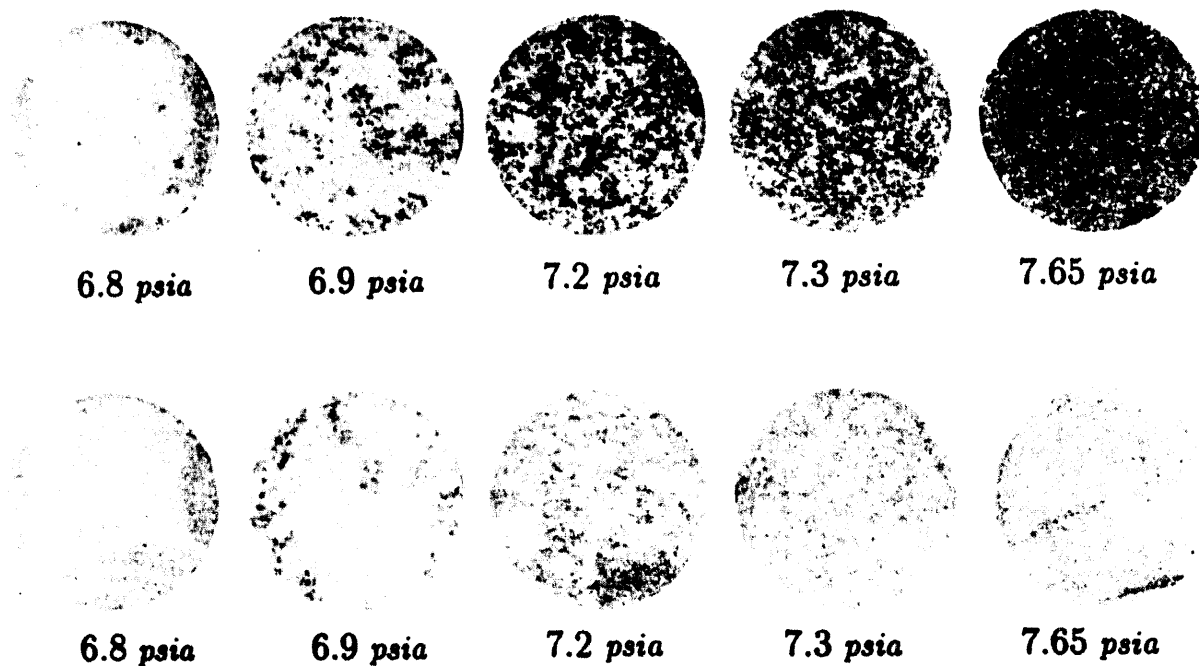


FIG. 19. Top and bottom axial quarter sections of Berea sandstone core partially saturated with a nonwetting fluid (Wood's metal alloy) at different equilibrium pressures, and solidified in place. The light phase is quartz grains and the dark phase is pores saturated with the alloy. The procedure allows for direct observation and analysis of the fluid distribution at a fixed pore pressure and saturation level. The sections reveal that the fluid distributions are composed of a set of imbibing clusters correlated in space.

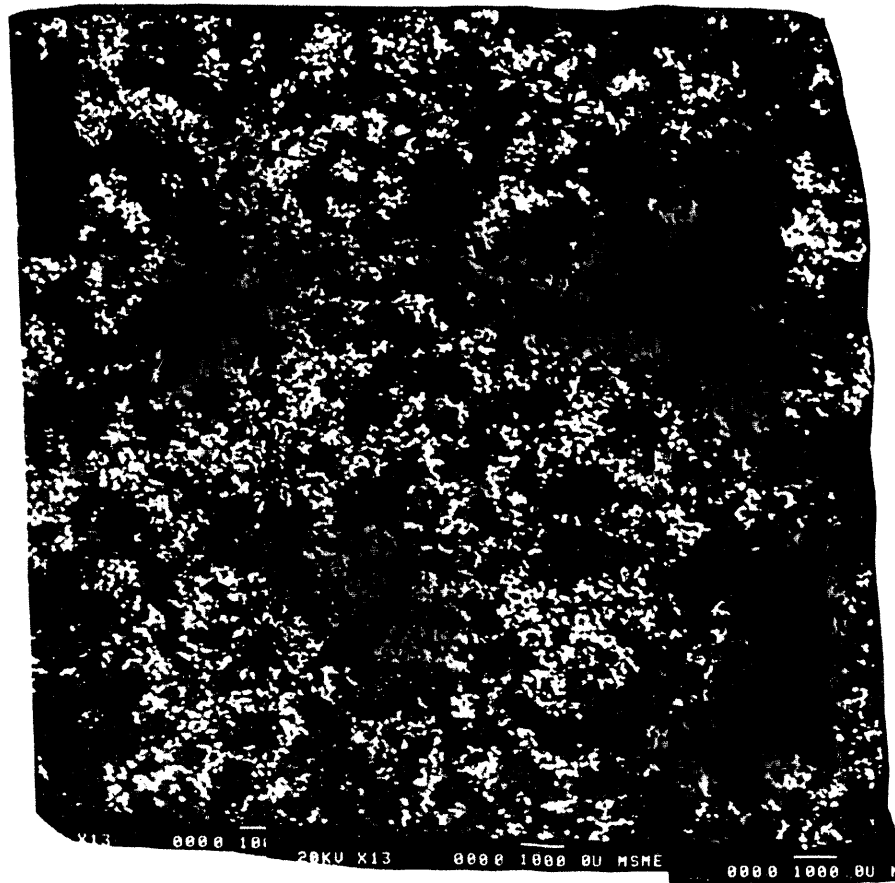


FIG. 20. SEM photomicrograph collage of a 1 in  $\times$  1 in Berea sandstone specimen partially saturated with approximately 30% Wood's metal at 7.3 psia equilibrium pressure. The rock is composed mainly of quartz grains (gray phase) and pore space that has been impregnated with Wood's metal (white phase) and epoxy (black phase) for imaging purposes.

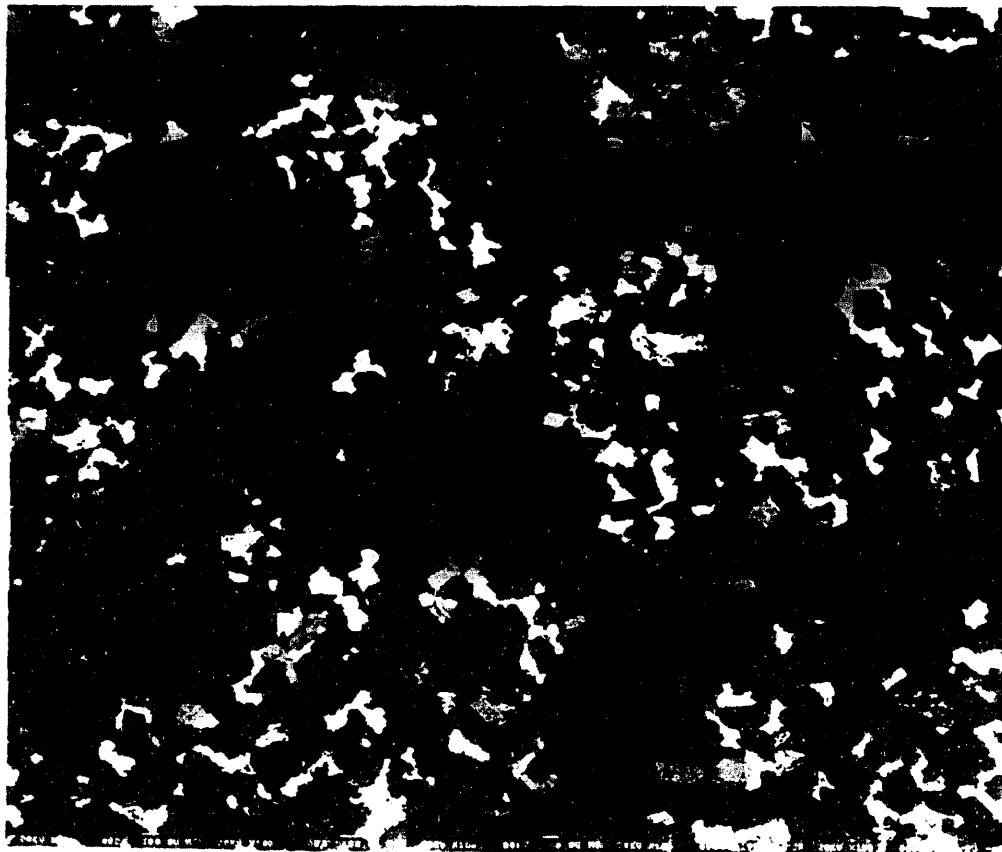
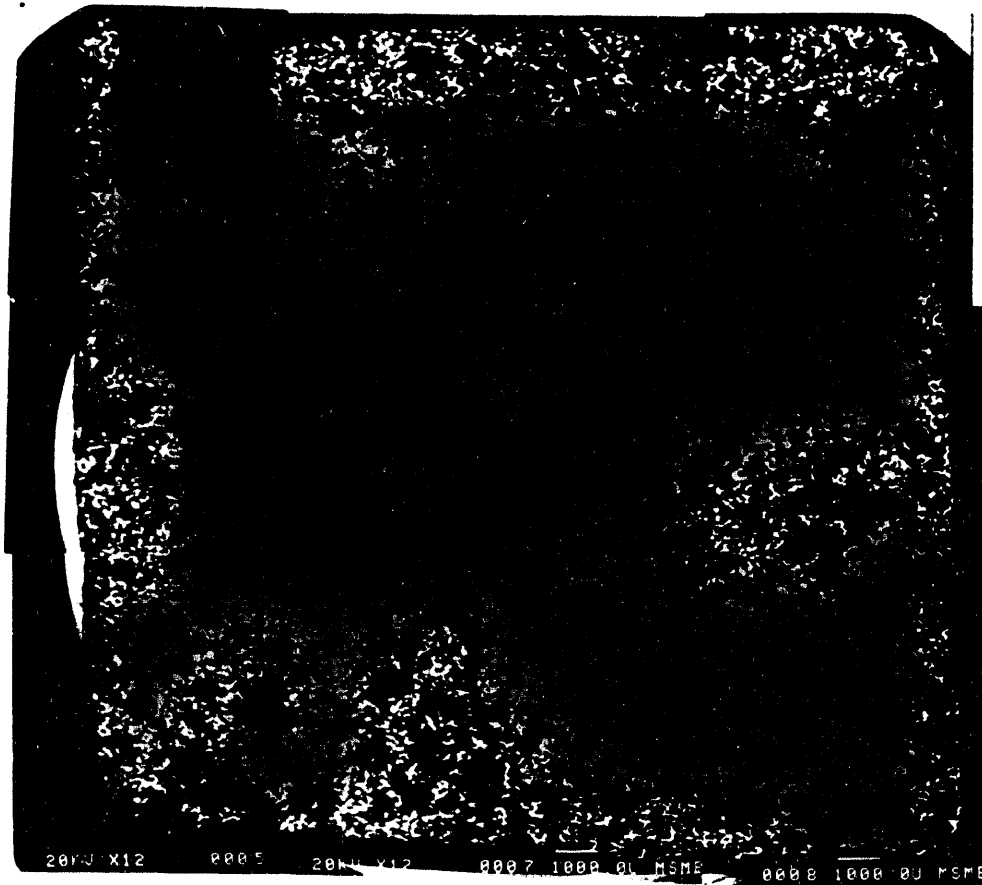


FIG. 21. SEM photomicrograph collage of an enlarged partial section obtained from a Berea sandstone sample partially saturated with approximately 30% Wood's metal (white phase) at 7.3 psia pressure shown in Fig. 20. Actual width of field is about 5 mm.



**FIG. 22.** SEM photomicrograph collage of a 1 in  $\times$  1 in Berea sandstone specimen partially saturated with approximately 50% Wood's metal at 8.5 psia equilibrium pressure. The rock is composed mainly of quartz grains (gray phase) and pore space that has been impregnated with Wood's metal (white phase) and epoxy (black phase) for imaging purposes.

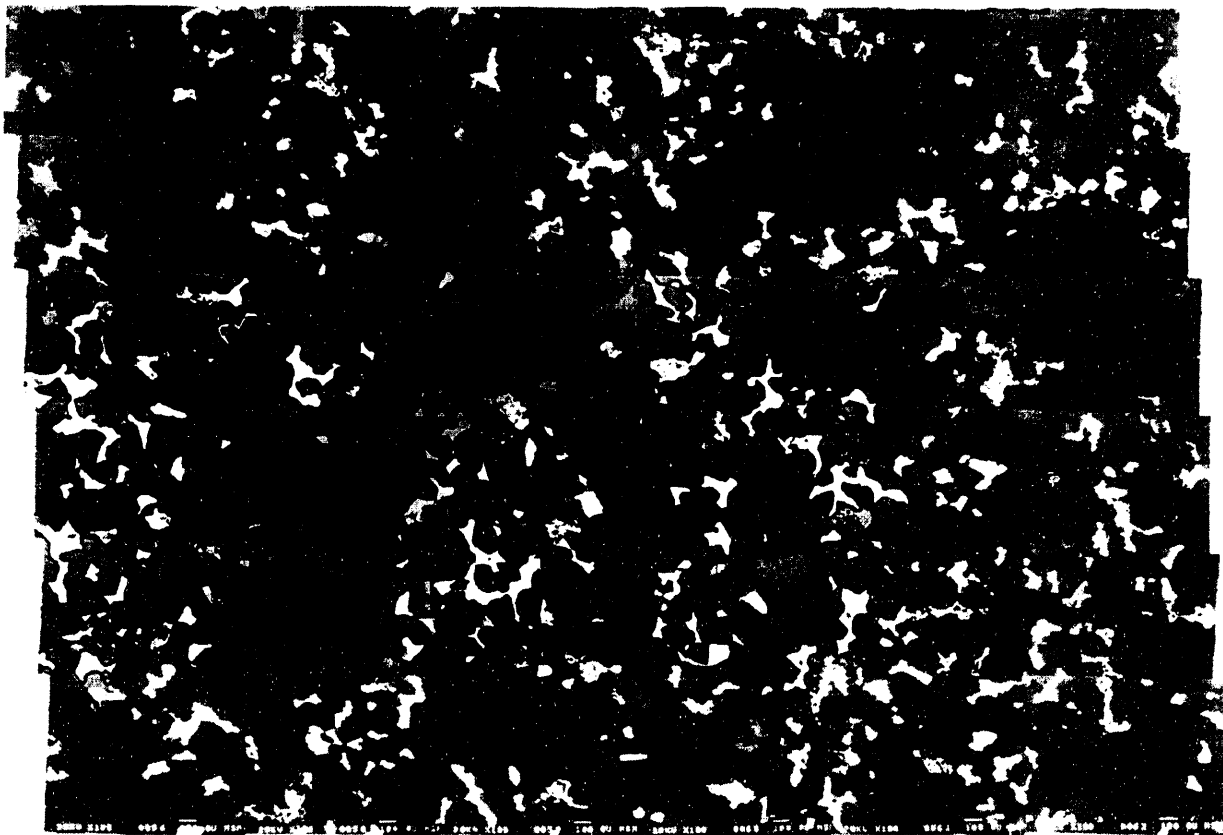


FIG. 23. SEM photomicrograph collage of an enlarged partial section obtained from a Berea sandstone sample partially saturated with approximately 50% Wood's metal (white phase) at 8.5 psia pressure shown in Fig. 22. Actual width of field is about 6 mm.

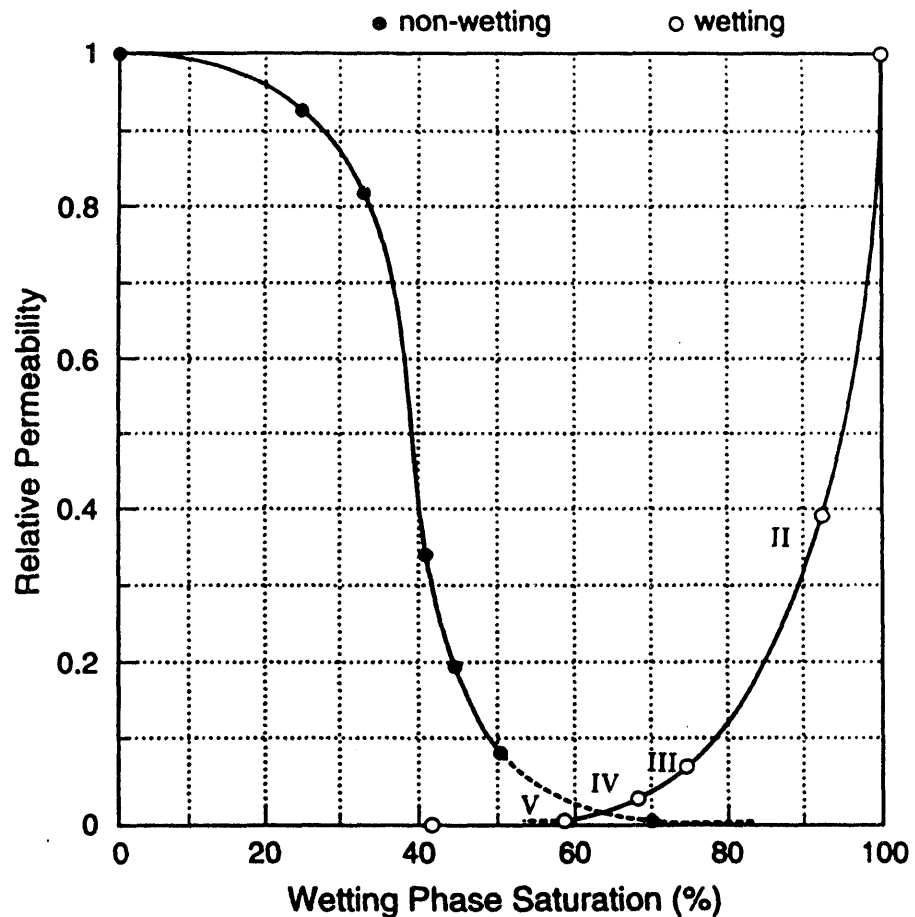


FIG. 24. Relative permeability vs. saturation curve for Berea sandstone using two fluids, serving as the wetting and nonwetting phases, that can be frozen in situ, one at a time. The effective permeability of the spaces not occupied by the wetting fluid (paraffin wax) and the nonwetting fluid (Wood's metal), respectively, have been measured at various saturations in Berea sandstone samples of absolute permeability of 600 md. The capillary pressures (in psia) for the points on the plot are II = 6.9, III = 7.2, IV = 7.3, and V = 7.7 psia.

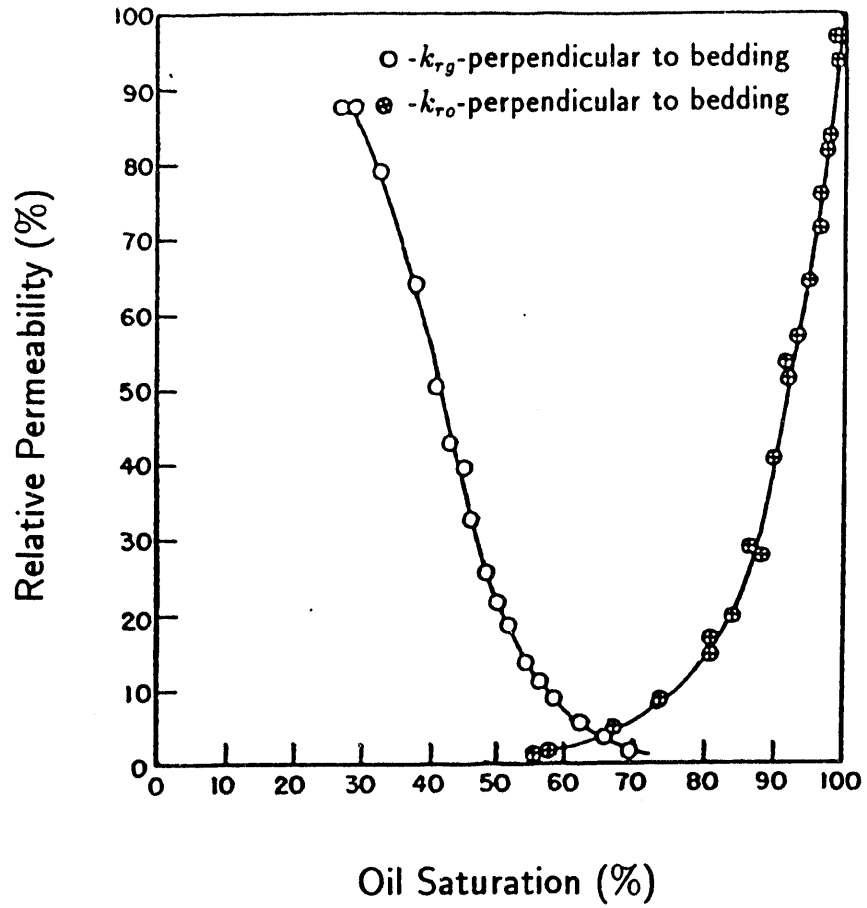


FIG. 25. Relative permeability vs. saturation curve for Berea sandstone measured by Corey and Rathjens<sup>[17]</sup> using oil and gas.

**DATE**

**FILMED**

*10/12/94*

**END**

